Supporting Information

Transformation and mobility of Cu, Zn, and Cr in sewage sludge during anaerobic digestion with pre- or inter-stage hydrothermal treatment

Qian Wang,[†] Chiqian Zhang,[‡] Haesung Jung,[†] Pan Liu,[†] Dhara Patel,[†] Spyros G. Pavlostathis,[‡] and Yuanzhi Tang[*,†,‡]

[†] School of Earth and Atmospheric Sciences, Georgia Institute of Technology, 311 Ferst Dr., Atlanta, GA 30332-0340, United States
[‡] School of Civil and Environmental Engineering, Georgia Institute of Technology, 311 Ferst Dr., Atlanta, GA 30332-0512, United States

*Corresponding author.
E-mail address: yuanzhi.tang@eas.gatech.edu
Phone: 404-894-3814

Total 25 pages
6 tables
12 figures

Text S1. Sequential chemical extraction (SCE)

Sequential extraction of raw sludge, hydrochars, and AD solids was performed using the three-stage Community Bureau of Reference (BCR) procedure.[1] Briefly, each solid sample (~ 0.25 g) was sequentially extracted by 20 mL of chemical solutions defined as: (1) acid soluble (0.11 M acetic acid for 16 h); (2) reducible (0.1 M hydroxylamine hydrochloride at pH 2.0 for 16 h); (3) oxidizable (4 mL 30% H_2O_2 for 16 h, air dried, then 1 M ammonium acetate at pH 2.0 for 16 h); and (4) residue (ashed at 550 °C in a muffle furnace, then digested by aqua regia). An aliquot of the extract from each step was diluted, mixed with scandium solution (an internal standard; final concentration at 25 ppb), and analyzed for element concentrations using inductively coupled plasma-mass spectrometry (ICP-MS). All extractions were performed in duplicate. The percentage of each fraction was calculated by metal concentration in the extract/residue divided by the total metal concentration, which was measured after aqua regia digestion of the unreacted solids.

Text S2. XAS analyses

X-ray absorption spectroscopy (XAS). Cu and Zn K-edge X-ray absorption near edge structure (XANES) spectra were collected using a 13-element Ge solid state detector at Beamline 4-1 at the Stanford Synchrotron Radiation Lightsource (SSRL; Menlo Park, CA, USA) and a Vortex detector at Beamline 12-BM at Advanced Photon Source (APS; Lemont, IL, USA). Freeze-dried solid samples were evenly dusted on a Scotch tape and mounted on the sample holder. Cu or Zn metal foils were used for energy calibration. Both fluorescence and transmission data were collected. The fluorescence data were used for the sludge related samples, and reference compounds used the transmission data.

Micro X-ray fluorescence (μ-XRF) imaging and μ-XANES. Synchrotron μ-XRF/XANES analyses were conducted on the dried solids at Beamline 2-3 at SSRL and Beamline 5-ID at National Synchrotron Light Source II (NSLS-II, Upton, NY, USA). Solid samples were dusted on a Kapton tape and mounted to the sample stage. Element maps were collected at an incident beam energy of 12 KeV with a beam size of 5×5 μm^2 (SSRL) or 10 KeV with a beam size of 1×1 μm^2 (NSLS-II). The software SMAK and PyXRF were used for processing SSRL and NSLS-II image data, respectively. Cr K-edge μ-XANES spectra were collected at selected hot spots. Cr foil was used for energy calibration. The μ-XANES data were processed using the same procedure as described for the bulk Cu and Zn XANES data.

LCF analyses of Cu, Zn, and Cr XANES data were performed at an energy region of -20 to +100 eV relative to the edge energy. LCF analyses of Cu and Zn EXAFS data were also conducted in the k^3 weighted χ-space (3 – 11.5 $Å^{-1}$). Energy shifts were not allowed during the LCF analyses.

Text S3. Changes in the total concentrations of Cu, Zn, and Cr

Regardless of the treatment sequence (HT-AD versus AD-HT-AD), the concentrations of Cu, Zn, and Cr in the process waters derived from HT or AD are all under 10 ppb, suggesting that heavy metals are retained in the solids. For HT-AD system, the concentrations of Cu, Zn, and Cr in the hydrochars increase with HT temperature as compared to raw sludge (Figure S3a and S3c). The enrichment of heavy metals in the hydrochars is due to the decreased solid mass from the conversion of organic matter to biogas and carbonization during HT.[2] The total concentrations of Cu and Cr in HT hydrochars and the subsequent AD solids are comparable. However, Zn concentrations is slightly higher in the AD solids than the HT hydrochars, especially for the sludge treated by low-temperature HT (i.e., 90 and 125 °C). This suggests that Cu and Cr are retained in

the solid phase during subsequent AD whereas Zn experienced some mobilization. For AD-HT-AD system, the total concentrations of Cu, Zn, and Cr in sample A15 increase as compared to raw sludge (Figure S3b and S3d), and further increase in the subsequent HT hydrochars and final AD solids.

Table S1. Sample label, chemical formula, and source of reference compounds used for linear combination fitting (LCF) analyses of Cu and Zn XANES data.

Element	Sample (label)	Synthesis or source	Reference
Cu	Cu_2S		*(3)*
	CuS		
	Cu-phosphate	$Cu_3(PO_4)_2$	
	Chalcopyrite	$CuFeS_2$, from Harvard University Mineralogical & Geological Museum	This work
	$Cu(OH)_2$		*(2)*
	Cu adsorbed on ferrihydrite (Cu_ad_Fhyd)	5 mM Cu^{2+} and 100 mg ferrihydrite in 20 mL solution with 10 mM NaCl, pH 6.0, 24 h, collected by 0.45 µm filtration	
	Cu-humic acid complex (Cu_Humic)	5 mM Cu^{2+} and 20 mg Elliot soil humic acid (IHSS) in 20 mL solution with 10 mM NaCl, pH 2.9, 24 h, collected by 0.45 µm filtration	
Zn	sphalerite	(Zn,Fe)S, Ward's Natural Science	*(2)*
	Zn adsorbed on ferrihydrite (Zn_ad_Fhyd)	5 mM Zn^{2+} and 100 mg ferrihydrite in 20 mL solution with 10 mM NaCl, pH 6.0, 24 h, collected by 0.45 µm filtration	
	Zn-humic acid complex (Zn_Humic)	5 mM Zn^{2+} and 10 mg Elliot soil humic acid (IHSS) in 20 mL solution with 10 mM NaCl, pH 3.2, 24 h, collected by 0.45 µm filtration	
	ZnS	Alfa Aesar	
	nano-ZnS	Synthesized following Le Bars et al.[4]	This work
	hopeite	$Zn_3(PO_4)_2{\cdot}4H_2O$	*(5)*
Cr	Cr(III)-humic complex (Cr(III)-humic)	Cr(III) complexing with peat humic acid	*(6)*
	Cr_2O_3	Alfa Aesar	This work
	$Cr(OH)_3$		*(7)*
	$Fe_{0.9}Cr_{0.1}(OH)_3$		*(8)*
	$Fe_{0.2}Cr_{0.8}(OH)_3$		
	fuchsite	$K(Al,Cr)_2(AlSi_3O_{10})(OH)_2$, Smithsonian	This work
	uvarovite	$Ca_3Cr_2(SiO_4)_3$, Smithsonian	
	K_2CrO_4		*(8)*
	$CaCrO_4$		*(9)*

Table S2. Relative abundance of Cu species determined from LCF analysis of Cu XANES spectra of the solid samples from HT-AD and AD-HT-AD systems. LCF derived errors are given in parentheses.

System	Sample	Cu species (%)				*R*-factor
		Cu_2S	CuS	chalcopyrite ($CuFeS_2$)	$Cu(OH)_2$	
HT-AD	raw sludge	-	61.3 (6.2)	28.3 (3.1)	10.4 (0.5)	0.0020
	A79	35.7 (3.4)	59.0 (4.7)	-	5.3 (0.4)	0.0009
	H90	8.9 (4.9)	74.4 (6.9)	10.4 (3.4)	6.3 (0.6)	0.0025
	H90A	23.7 (3.1)	71.3 (4.3)	-	5.0 (0.4)	0.0007
	H155	7.7 (4.8)	72.4 (6.7)	13.2 (3.4)	6.7 (0.6)	0.0024
	H155A	23.8 (3.3)	72.4 (4.7)	-	3.8 (0.4)	0.0009
	H185	11.2 (7.0)	66.0 (9.7)	15.1 (4.8)	7.7 (0.8)	0.0051
	H185A	8.0 (2.1)	92.0 (0.8)	-	-	0.0012
AD-HT-AD	raw sludge	-	61.3 (6.2)	28.3 (3.1)	10.4 (0.5)	0.0020
	A15	-	61.5 (6.1)	29.0 (3.0)	9.5 (0.5)	0.0019
	A89	44.7 (3.3)	55.3 (4.6)	-	-	0.0008
	AH90	-	57.5 (6.3)	32.7 (3.1)	9.8 (0.5)	0.0020
	AH90A	34.2 (3.6)	61.4 (5.0)	-	4.4 (0.5)	0.0010
	AH125	-	55.8 (6.6)	34.2 (3.3)	10.0 (0.5)	0.0022
	AH125A	35.9 (4.6)	60.0 (4.6)	-	4.1 (0.4)	0.0008
	AH155	-	59.3 (7.6)	32.9 (3.7)	7.8 (0.7)	0.0031
	AH155A	21.7 (3.1)	74.9 (4.4)	-	3.4 (0.4)	0.0008
	AH185	-	53.1 (5.9)	39.1 (2.9)	7.8 (0.5)	0.0018
	AH185A	-	81.7 (4.4)	14.6 (2.1)-	3.7 (0.4)	0.0008

Table S3. Relative abundance of Cu species determined from LCF analysis of Cu EXAFS spectra of the solid samples from HT-AD and AD-HT-AD systems. LCF derived errors are given in parentheses.

System	Sample	Cu species (%)				*R*-factor
		Cu_2S	CuS	chalcopyrite ($CuFeS_2$)	$Cu(OH)_2$	
HT-AD	raw sludge	-	-	86.5 (5.2)	13.5 (4.2)	0.2463
	A79	54.6 (16.2)		32.6 (12.4)	12.8 (3.8)	0.2662
	H90	-	-	79.3 (5.1)	20.7 (4.2)	0.2504
	H90A	42.8 (14.5)	4.0 (11.5)	38.0 (11.2)	15.2 (3.3)	0.2170
	H155	-	-	82.6 (7.1)	17.4 (5.8)	0.3923
	H155A	14.8 (15.3)	41.9 (12.2)	29.9 (11.9)	13.4 (3.5)	0.2299
	H185	-	-	77.3 (5.2)	22.7 (6.6)	0.4602
	H185A	-	17.4 (13.5)	61.5 (13.2)	21.1 (4.0)	0.2401
AD-HT-AD	raw sludge	-	-	86.5 (5.2)	13.5 (4.2)	0.2463
	A15	-	-	76.6 (4.2)	23.4 (3.4)	0.1819
	A89	40.9 (14.0)	23.8 (11.1)	19.9 (10.8)	15.4 (3.1)	0.2173
	AH90	-	-	82.2 (4.2)	17.8 (3.4)	0.1907
	AH90A	28.3 (15.3)	20.9 (12.0)	32.9 (11.7)	17. 9 (3.5)	0.2323
	AH125	-	-	79.2 (5.1)	20.8 (4.1)	0.2473
	AH125A	26.7 (12.6)	19.5 (9.9)	44.2 (9.7)	9.6 (2.9)	0.1626
	AH155	-	-	88.3 (6.8)	11.7 (5.5)	0.3653
	AH155A	15.1 (14.4)	23.0 (11.5)	49.6 (11.1)	12.3 (3.3)	0.1962
	AH185	-	-	85.3 (5.3)	14.7 (4.3)	0.2618
	AH185A	9.2 (12.4)	32.5 (9.8)	47.6 (9.5)	10.7 (2.7)	0.1554

Table S4. Relative abundance of Zn species determined from LCF analysis of Zn XANES spectra of the solid samples from HT-AD and AD-HT-AD systems. LCF derived errors are given in parentheses.

System	Sample	Zn species (%)				*R*-factor
		nano-ZnS	sphalerite ((Zn, Fe)S)	Zn_ad_Fhyd	Zn_humic	
HT-AD	raw sludge	63.2 (3.5)	31.1 (3.3)	5.7 (0.6)	-	0.0008
	A79	48.8 (3.2)	19.5 (3.0)	31.7 (0.5)	-	0.0006
	H90	61.2 (2.7)	31.8 (2.6)	7.0 (0.5)	-	0.0005
	H90A	35.9 (3.2)	25.0 (3.4)	21.1 (2.0)	18.0 (1.4)	0.0004
	H155	59.6 (4.1)	35.1 (3.8)	5.3 (0.7)	-	0.0010
	H155A	33.5 (0.7)	30.0 (0.4)	23.8 (1.8)	12.7 (1.2)	0.0005
	H185	57.8 (4.2)	36.7 (3.9)	5.5 (0.7)	-	0.0011
	H185A	25.0 (3.4)	37.4 (3.6)	18.2 (2.2)	19.4 (1.5)	0.0006
AD-HT-AD	raw sludge	63.2 (3.5)	31.1 (3.3)	5.7 (0.6)	-	0.0008
	A15	58.0 (3.1)	32.3 (2.9)	9.7 (0.5)	-	0.0006
	A89	45.2 (2.6)	27.8 (2.8)	14.9 (1.7)	12.1 (1.2)	0.0004
	AH90	57.2 (3.1)	35.9 (2.9)	6.9 (0.5)	-	0.0006
	AH90A	40.8 (3.2)	35.7 (3.4)	12.1 (2.0)	11.4 (1.4)	0.0005
	AH125	57.2 (3.1)	35.9 (2.9)	6.9 (0.5)	-	0.0006
	AH125A	35.5 (3.4)	31.7 (3.6)	14.3 (2.1)	18.5 (1.5)	0.0005
	AH155	54.1 (3.8)	40.2 (3.5)	5.7 (0.6)	-	0.0009
	AH155A	25.0 (5.2)	37.4 (5.5)	14.3 (3.2)	23.3 (2.3)	0.0011
	AH185	50.0 (3.6)	42.2 (3.4)	7.8 (0.6)	-	0.0008
	AH185A	20.2 (3.7)	41.2 (3.9)	24.9 (2.3)	13.7 (1.6)	0.0006

Table S5. Relative abundance of Zn species determined from LCF analysis of Zn EXAFS spectra of the solid samples from HT-AD and AD-HT-AD systems. LCF derived errors are given in parentheses.

System	Sample	Zn species (%)				*R*-factor
		nano-ZnS	sphalerite ((Zn, Fe)S)	Zn_ad_Fhyd	Zn_humic	
HT-AD	raw sludge	92.9 (5.4)	7.1 (7.6)	-	-	0.0912
	A79	58.6 (7.0)	18.1 (4.3)	23.3 (4.8)	-	0.1395
	H90	89.1 (4.0)	10.9 (4.8)	-	-	0.0753
	H90A	45.6 (6.0)	16.4 (3.7)	25.2 (6.4)	12.8 (6.6)	0.1282
	H155	84.2 (4.5)	15.8 (5.4)	-	-	0.0985
	H155A	53.1 (6.7)	12.1 (4.1)	22.5 (7.1)	12.3 (7.4)	0.1482
	H185	78.1 (3.9)	21.9 (2.8)	-	-	0.0801
	H185A	49.8 (5.5)	12.5 (3.4)	26.3 (5.9)	11.4 (6.0)	0.1104
AD-HT-AD	raw sludge	92.9 (5.4)	7.1 (7.6)	-	-	0.0912
	A15	83.5 (4.9)	16.5 (3.6)	-	-	0.1279
	A89	64.5 (8.4)	35.5 (8.9)	-	-	0.2394
	AH90	71.1 (5.3)	17.6 (3.5)	11.3 (3.9)	-	0.1049
	AH90A	54.1 (4.5)	10.9 (2.7)	22.1 (4.7)	12.9 (5.0)	0.0739
	AH125	75.5 (4.8)	12.7 (3.1)	11.8 (3.6)	-	0.0896
	AH125A	64.0 (5.1)	16.9 (3.1)	9.3 (5.5)	9.8 (5.6)	0.0796
	AH155	74.9 (3.7)	25.1 (2.7)	-	-	0.0712
	AH155A	38.5 (5.6)	15.4 (3.4)	10.8 (5.8)	35.3 (6.1)	0.1098
	AH185	76.3 (6.5)	23.7 (4.3)	-	-	0.1340
	AH185A	40.8 (5.3)	17.3 (3.3)	20.0 (5.6)	21.9 (5.9)	0.0872

Table S6. Relative abundance of different Cr species determined from LCF of Cr K-edge μ-XANES data of the solid samples from HT-AD and AD-HT-AD systems. LCF derived errors are given in parentheses.

System	Sample		Cr species (%)							*R*-factor
			Cr(III)-humic	$Fe_{0.9}Cr_{0.1}(OH)_3$	$Fe_{0.2}Cr_{0.8}(OH)_3$	$Cr(OH)_3$	Cr_2O_3	fuchsite	uvarovite	
HT-AD	raw sludge	Spot 1	93.1 (0.5)	6.9 (0.4)	-	-	-	-	-	0.0191
		Spot 2	87.6 (8.0)	12.4 (0.4)	-	-	-	-	-	0.0189
	A79	Spot 1	40.4 (10.0)	27.5 (7.0)	32.1 (7.0)	-	-	-	-	0.0338
		Spot 2	51.7 (2.8)	-	-	10.8 (3.3)	37.6 (4.2)	-	-	0.0031
	H90	Spot 1	17.6 (8.3)	49.9 (10.4)	-	-	32.5 (8.2)	-	-	0.0129
		Spot 2	21.2 (1.3)	10.8 (2.8)	20.0 (1.9)	-	-	48.0 (4.5)	-	0.0181
	H90A	Spot 1	11.8 (9.5)	22.0 (9.0)	-	66.2 (5.5)	-	-	-	0.0218
		Spot 2	70.3 (8.2)	19.4 (9.2)	-	-	-	10.3 (5.9)	-	0.0349
	H155	Spot 1	-	68.2 (3.2)	-	-	17.3 (5.0)	14.5 (3.2)	-	0.0098
		Spot 2	-	38.5 (9.3)	-	-	21.6 (8.7)	39.9 (6.9)	-	0.0214
	H155A	Spot 1	39.0 (10.0)	5.9 (4.4)	-	55.1 (7.0)	-	-	-	0.0202
		Spot 2	-	36.9 (8.5)	-	-	63.1 (9.1)	-	-	0.0413
	H185	Spot 1	-	-	-	-	70.7 (7.1)	-	29.3 (4.1)	0.0731
		Spot 2	-	-	-	-	75.5 (9.9)	-	24.5 (9.7)	0.0387
	H185A	Spot 1	-	54.2 (6.8)	-	-	45.8 (10.1)	-	-	0.0163
		Spot 2	-	-	79.6 (8.5)	-	20.4 (8.6)	-	-	0.0112

continued

System	Sample		Cr species (%)							*R*-factor
			Cr(III)-humic	$Fe_{0.9}Cr_{0.1}(OH)_3$	$Fe_{0.2}Cr_{0.8}(OH)_3$	$Cr(OH)_3$	Cr_2O_3	fuchsite	uvarovite	
AD-HT-AD	raw sludge	Spot 1	93.1 (0.5)	6.9 (0.4)	-	-	-	-	-	0.0191
		Spot 2	87.6 (8.0)	12.4 (0.4)	-	-	-	-	-	0.0189
	A15	Spot 1	-	67.7 (9.5)	-	32.3 (4.9)	-	-	-	0.0141
		Spot 2	81.9 (5.6)	-	-	18.1 (5.7)	-	-	-	0.0160
	A89	Spot 1	53.9 (8.8)	-	-	46.1 (9.0)	-	-	-	0.0311
		Spot 2	-	75.7 (3.6)	-	24.3 (3.6)	-	-	-	0.0099
		Spot 3	-	61.3 (1.4)	13.3 (3.6)	25.4 (3.8)	-	-	-	0.0050
	AH90	Spot 1	64.2 (6.3)	-	-	-	-	35.8 (7.1)	-	0.0468
		Spot 2	51.8 (7.3)	-	-	48.2 (7.6)	-	-	-	0.0316
	AH90A	Spot 1	-	-	55.2 (4.6)	44.8 (1.3)	-	-	-	0.0392
		Spot 2	-	-	52.9 (7.8)	47.1 (7.8)	-	-	-	0.0232
	AH125	Spot 1	-	-	-	-	12.0 (4.0)	88.0 (4.0)	-	0.0159
		Spot 2	-	-	-	-	7.0 (3.3)	93.0 (2.6)	-	0.0372
	AH125A	Spot 1	-	-	55.2 (4.6)	44.8 (1.3)	-	-	-	0.0147
		Spot 2	-	-	44.7 (7.8)	17.9 (3.3)	37.4 (3.4)	-	-	0.0267
	AH155	Spot 1	-	-	-	26.2 (7.5)	-	73.8 (9.5)	-	0.0136
		Spot 2	-	-	-	31.7 (7.1)	5.2 (6.9)	63.1 (9.1)	-	0.0135
	AH155A	Spot 1	-	-	-	91.6 (9.0)	8.4 (9.1)	-	-	0.0317
		Spot 2	-	-	-	94.9 (4.7)	5.1 (4.8)	-	-	0.0144
	AH185	Spot 1	-	-	-	-	20.4 (7.6)	-	79.6 (7.5)	0.0391
		Spot 2	-	-	-	-	66.9 (4.1)	-	33.1 (5.0)	0.0654
	AH185A	Spot 1	-	14.0 (7.1)	-	86.0 (4.8)	-	-	-	0.0101
		Spot 2	-	-	34.0 (9.1)	66.0 (8.3)	-	-	-	0.0427

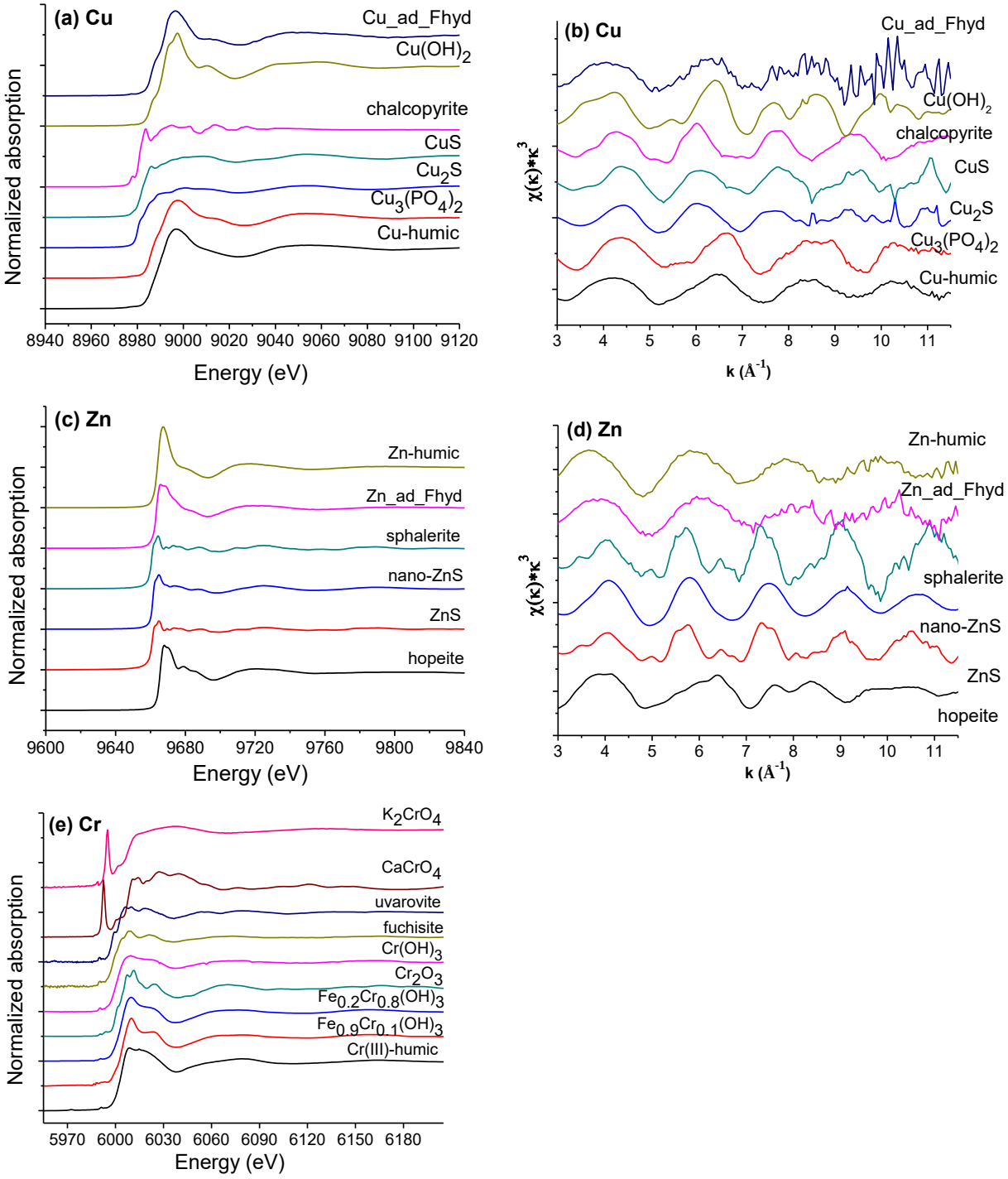

Figure S1. Cu, Zn, and Cr XAS spectra of the reference compounds listed in Table S1. (a) and (b) Cu XANES and corresponding EXAFS spectra, respectively; (c) and (d) Zn XANES and corresponding EXAFS spectra, respectively; (e) Cr XANES spectra.

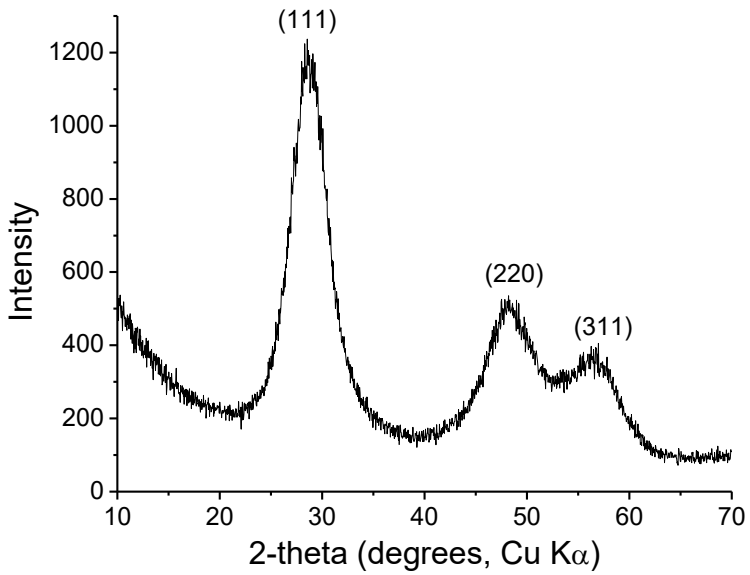

Figure S2. X-ray diffraction pattern of nano-ZnS.

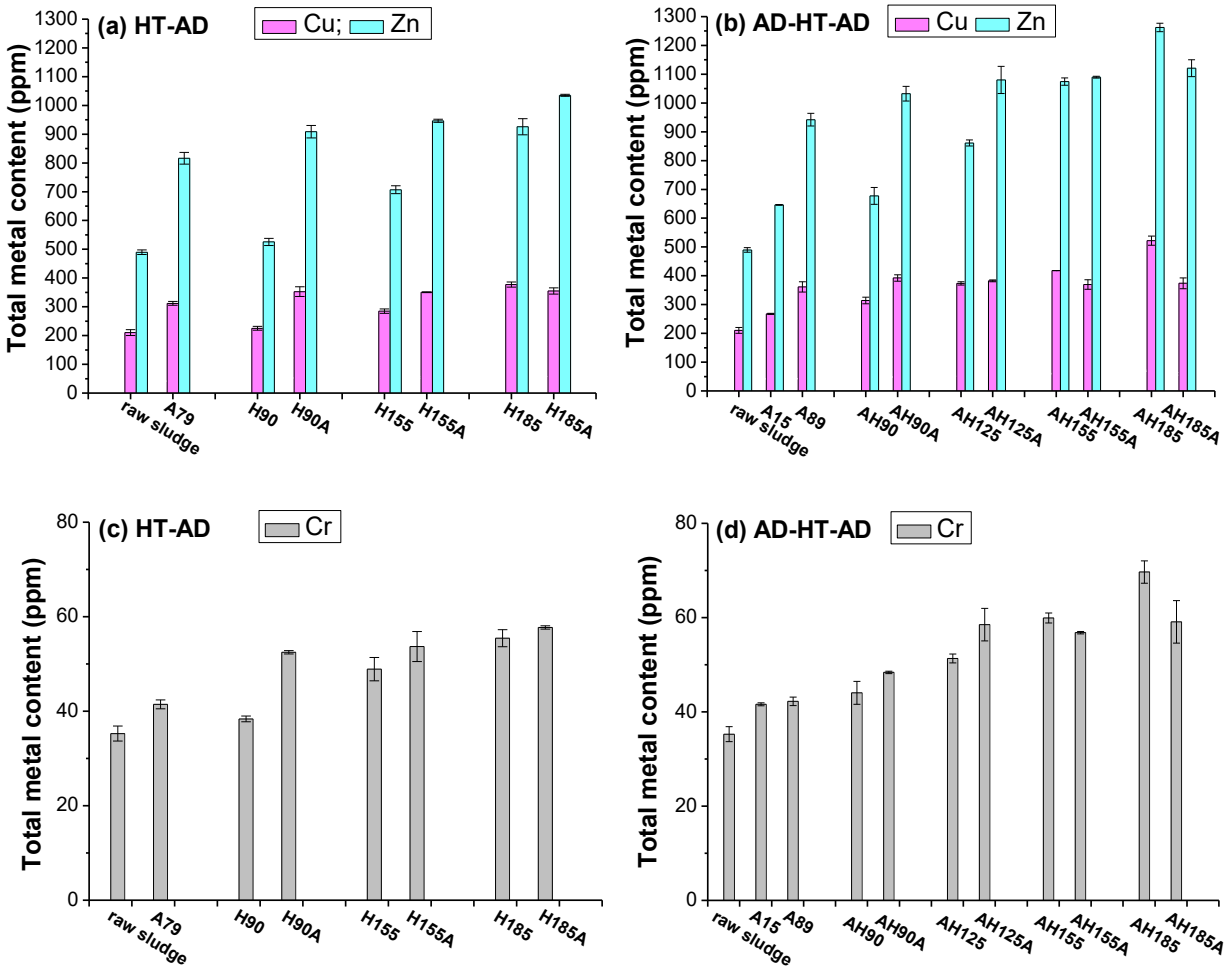

Figure S3. Total contents of Cu, Zn, and Cr in raw sludges, hydrochars, and AD solids from HT-AD (a and c) and AD-HT-AD (b and d) systems. Error bars indicate the standard deviation of measurements (n = 4).

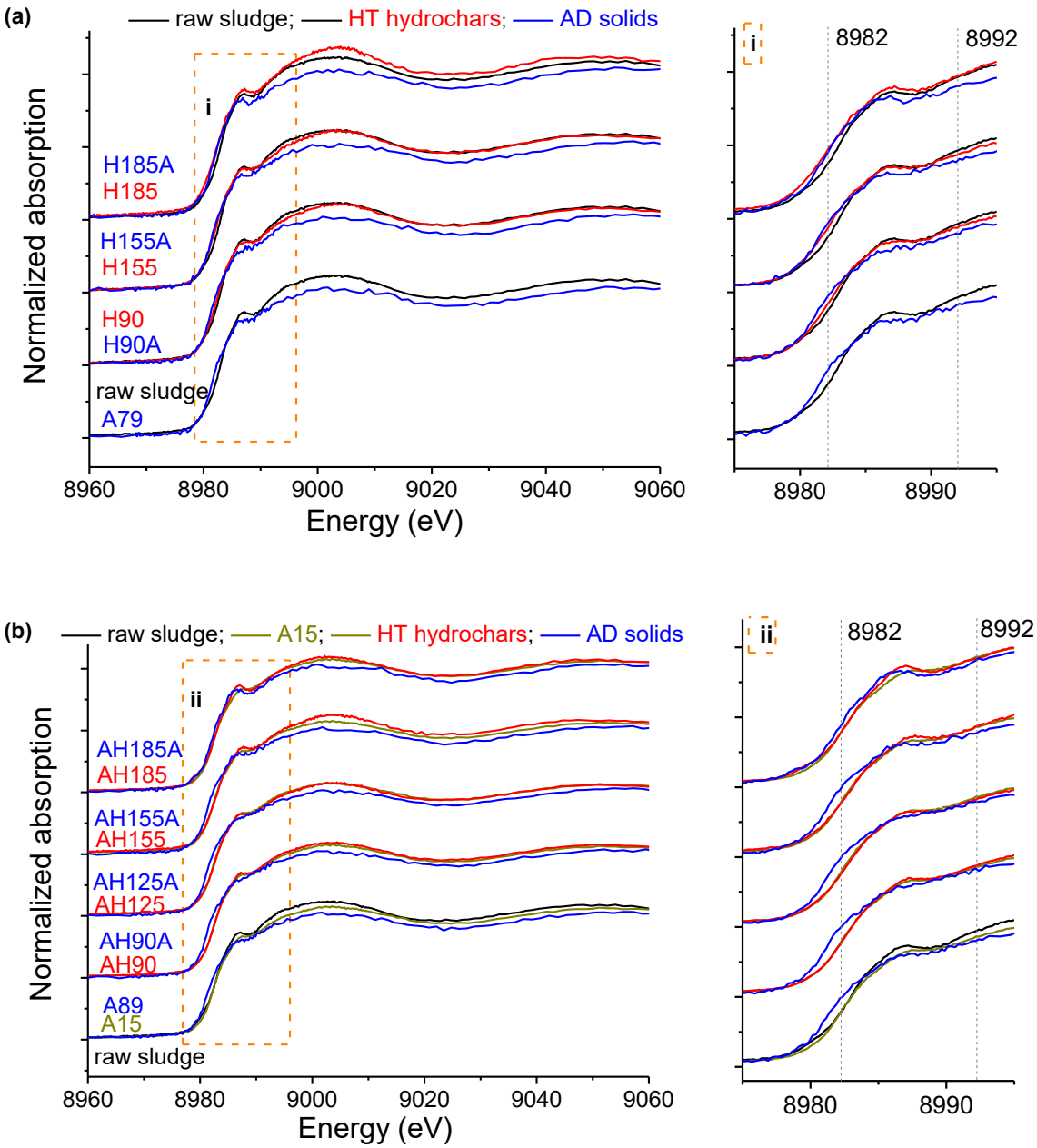

Figure S4. Cu K-edge XANES spectra of raw sludge, HT hydrochars, and AD solids from (a) HT-AD system and (b) AD-HT-AD system. Black, magenta, red, and blue lines are for raw sludge, A15, HT hydrochars, and AD solids, respectively. Right panels are zoomed views of edge features highlighted by dashed lines in left panels.

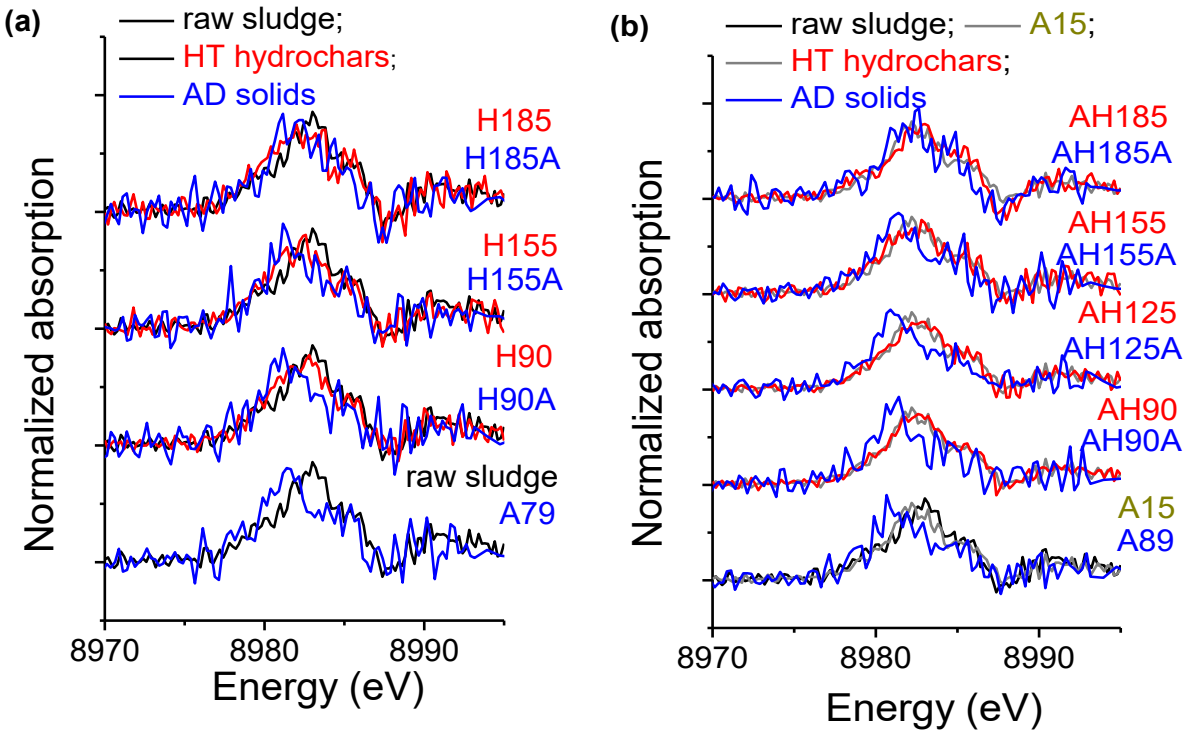

Figure S5. The first derivative of Cu K-edge XANES spectra of raw sludge, HT hydrochars, and AD solids from (a) HT-AD system and (b) AD-HT-AD system. Black, magenta, red, and blue lines are for raw sludge, A15, HT hydrochars, and AD solids, respectively.

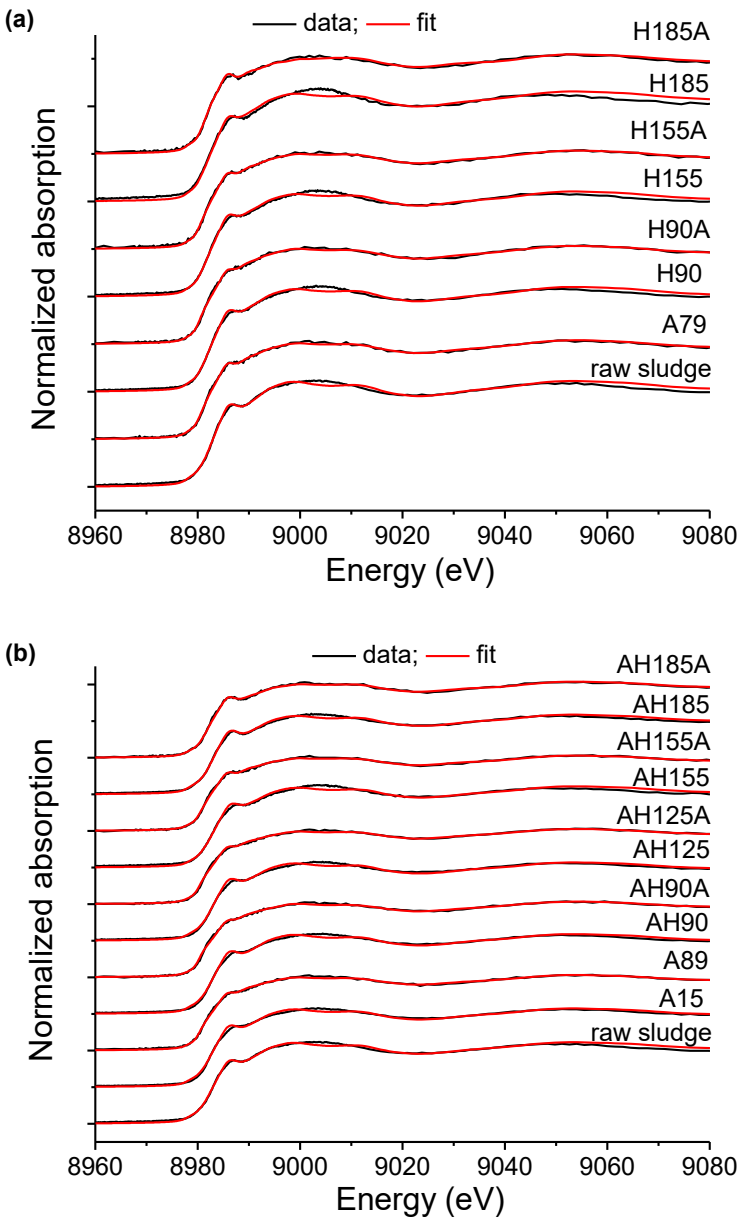

Figure S6. Results of LCF of Cu K-edge XANES of raw sludge, HT hydrochars, and AD solids from (a) HT-AD and (b) AD-HT-AD systems. Raw and fitted data are in black and red lines, respectively.

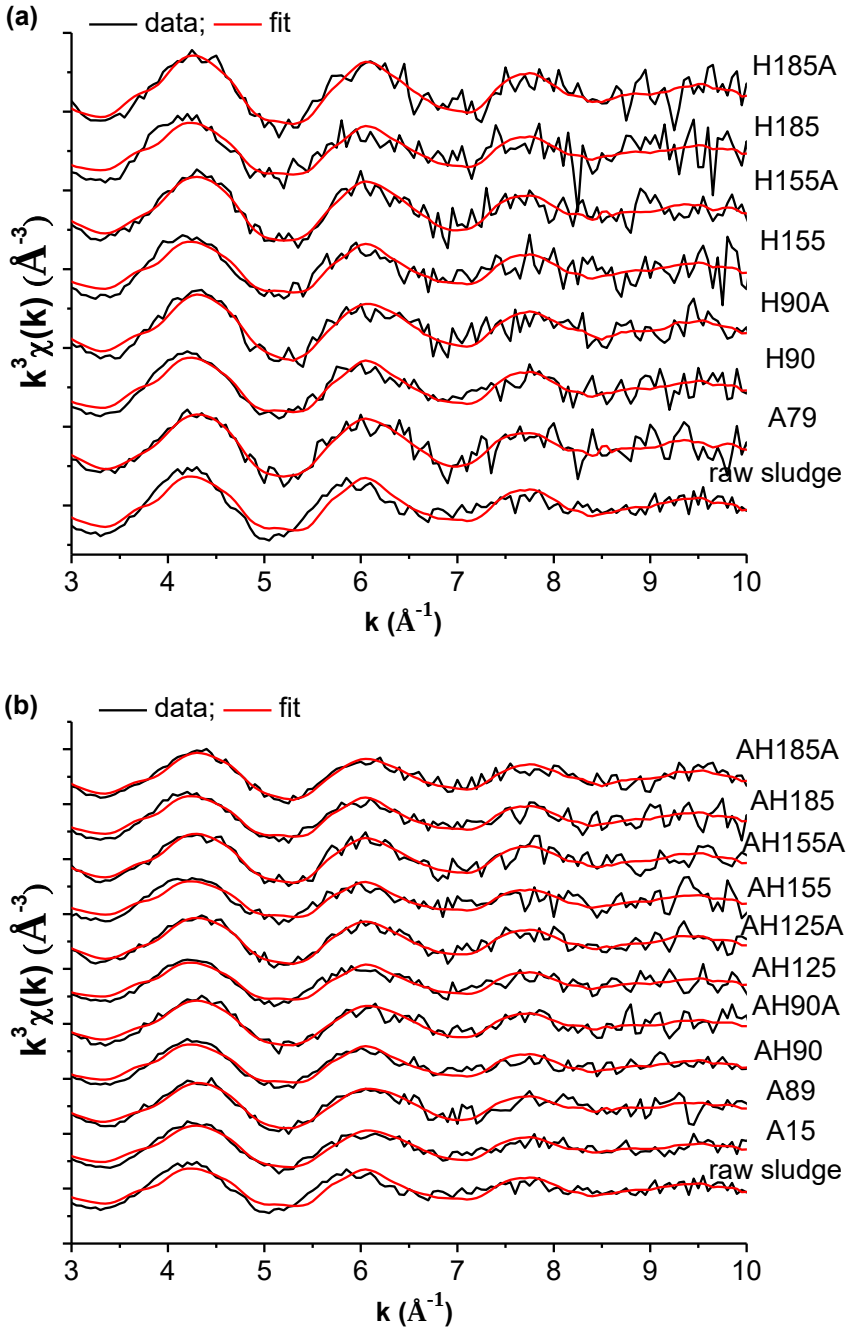

Figure S7. Results of LCF of Cu k^3-weighted EXAFS spectra of raw sludge, HT hydrochars, and AD solids from (a) HT-AD and (b) AD-HT-AD systems. Raw and LCF fitted data are shown in black and red lines, respectively.

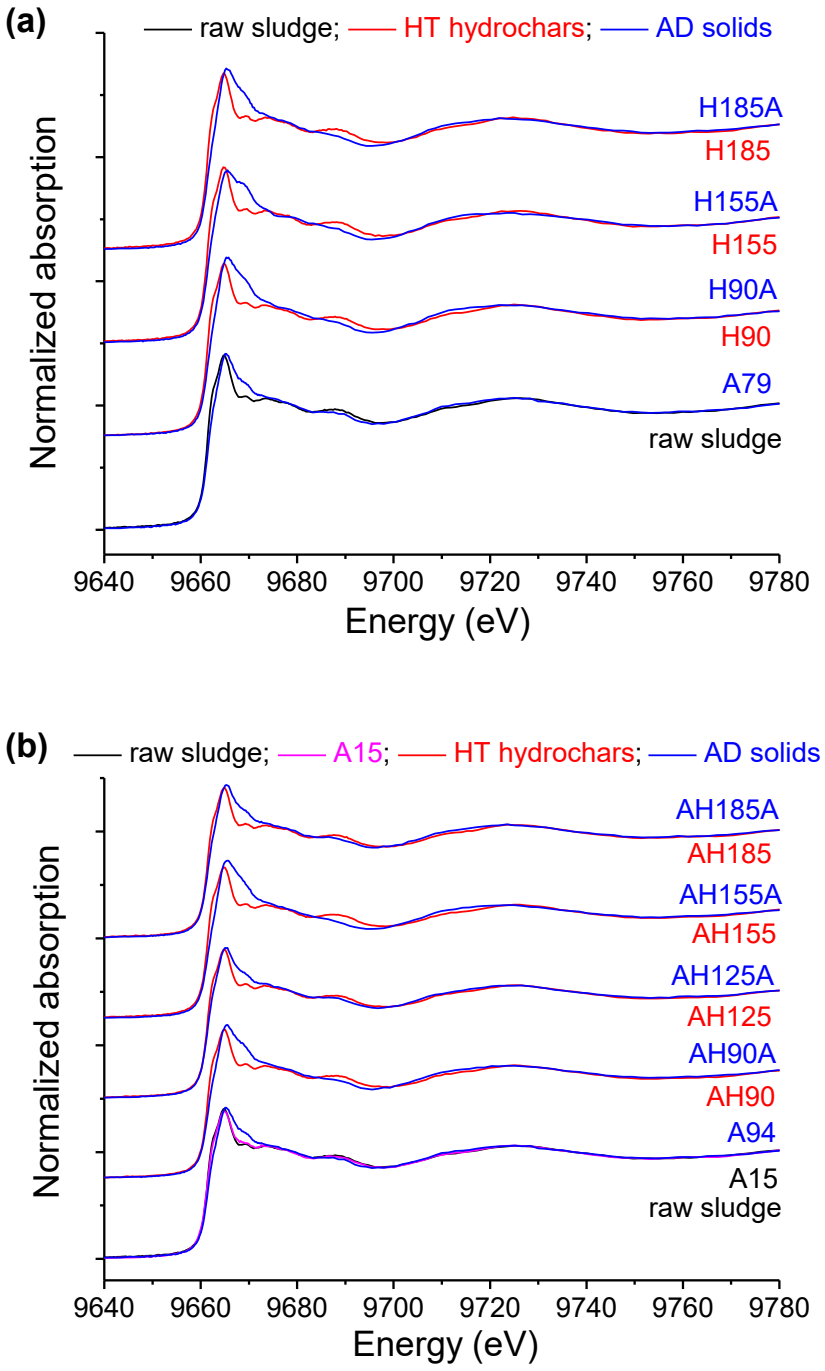

Figure S8. Zn K-edge XANES spectra of raw sludge, HT hydrochars, and AD solids from (a) HT-AD and (b) AD-HT-AD systems. Black, magenta red, and blue lines are for samples raw sludge, A15, HT hydrochars, and AD solids, respectively.

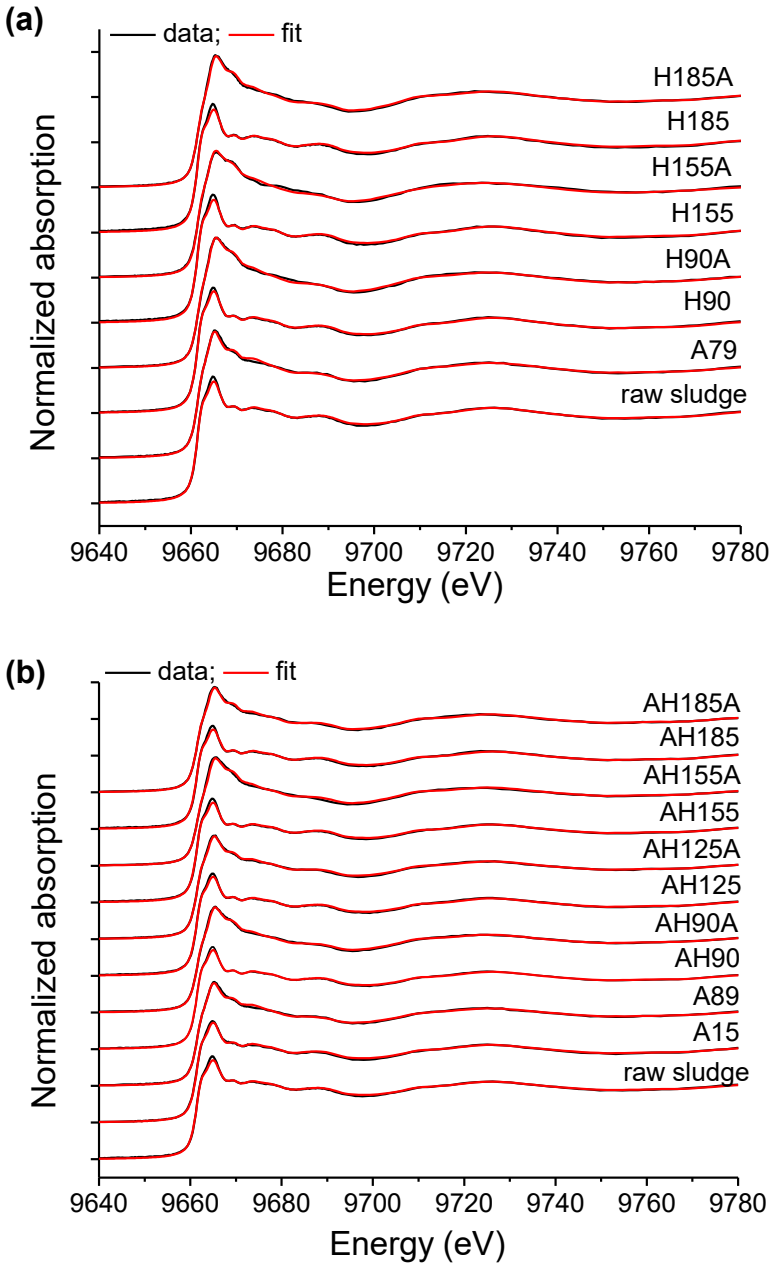

Figure S9. Linear combination fitting (LCF) of Zn K-edge XANES spectra of raw sludge, HT hydrochars, and AD solids from (a) HT-AD and (b) AD-HT-AD systems. Raw and LCF fitted data are shown in black and red lines, respectively.

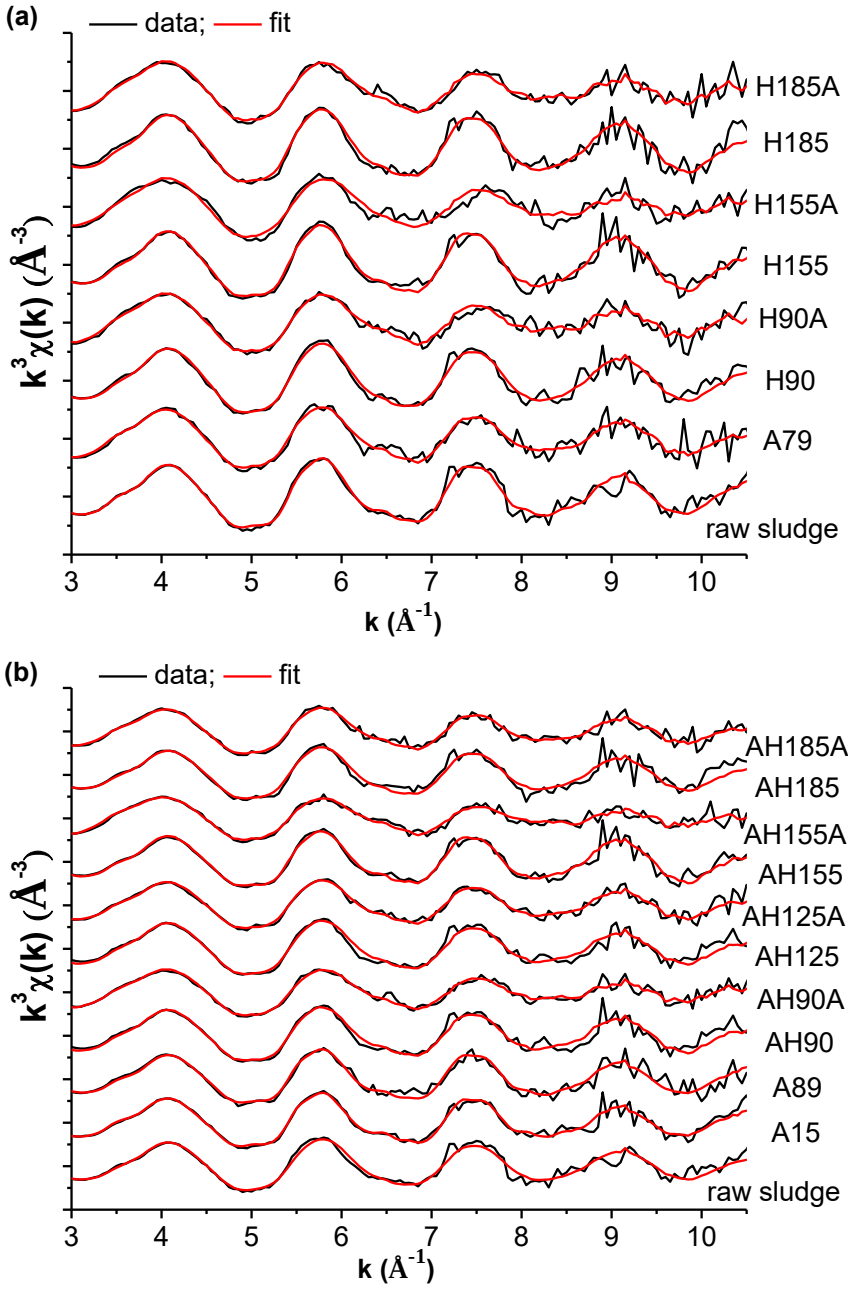

Figure S10. Results of LCF of Zn k^3-weighted EXAFS spectra of raw sludge, HT hydrochars, and AD solids from (a) HT-AD and (b) AD-HT-AD systems. Raw and LCF fitted data are shown in black and red lines, respectively.

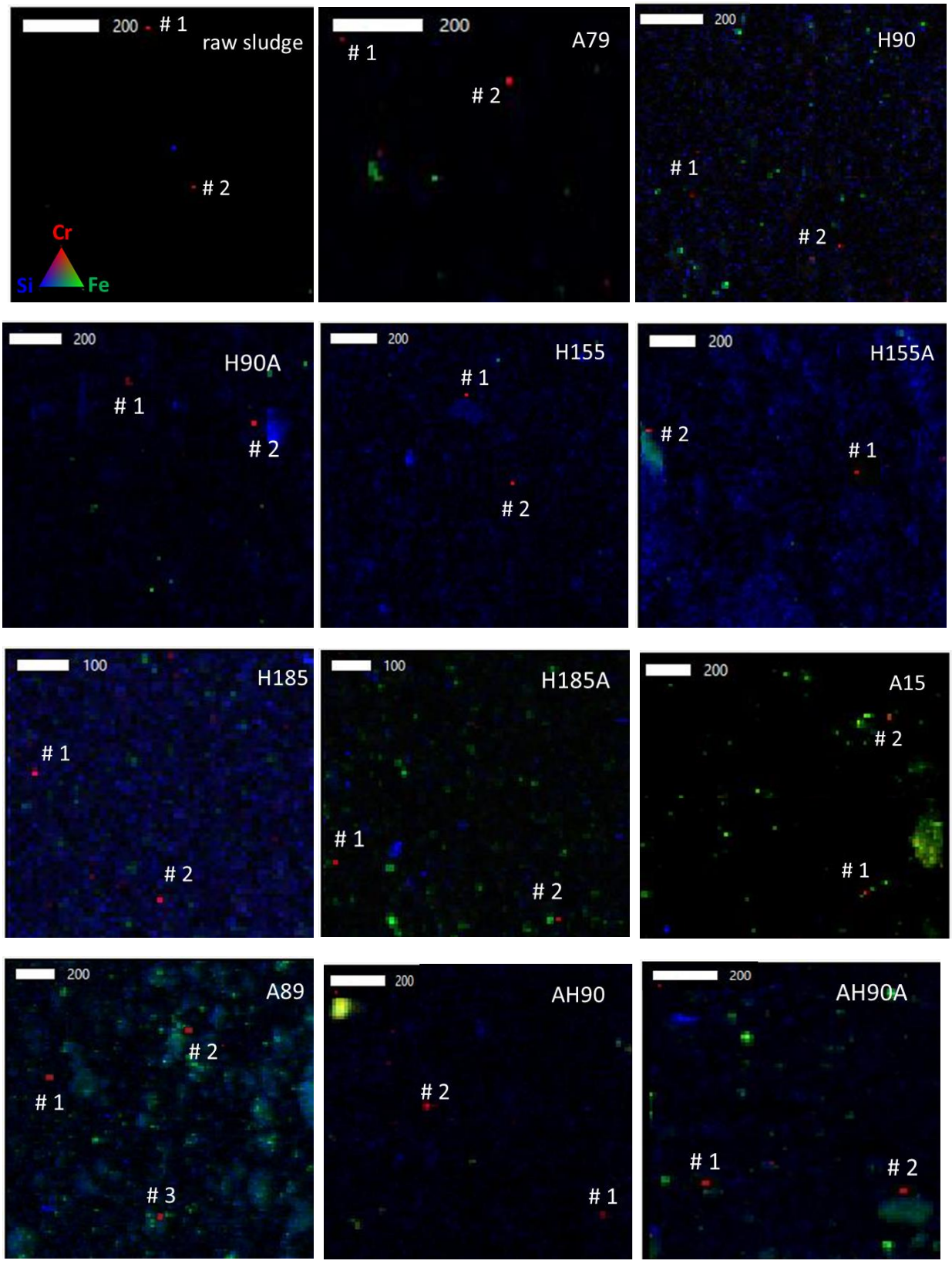
200
1
raw sludge
2
Cr
Si
Fe
200
A79
1
2
200
H90
1
2
200
H90A
1
2
200
H155
1
2
200
H155A
2
1
100
H185
1
2
100
H185A
1
2
200
A15
2
1
200
A89
2
1
3
200
AH90
2
1
200
AH90A
1
2

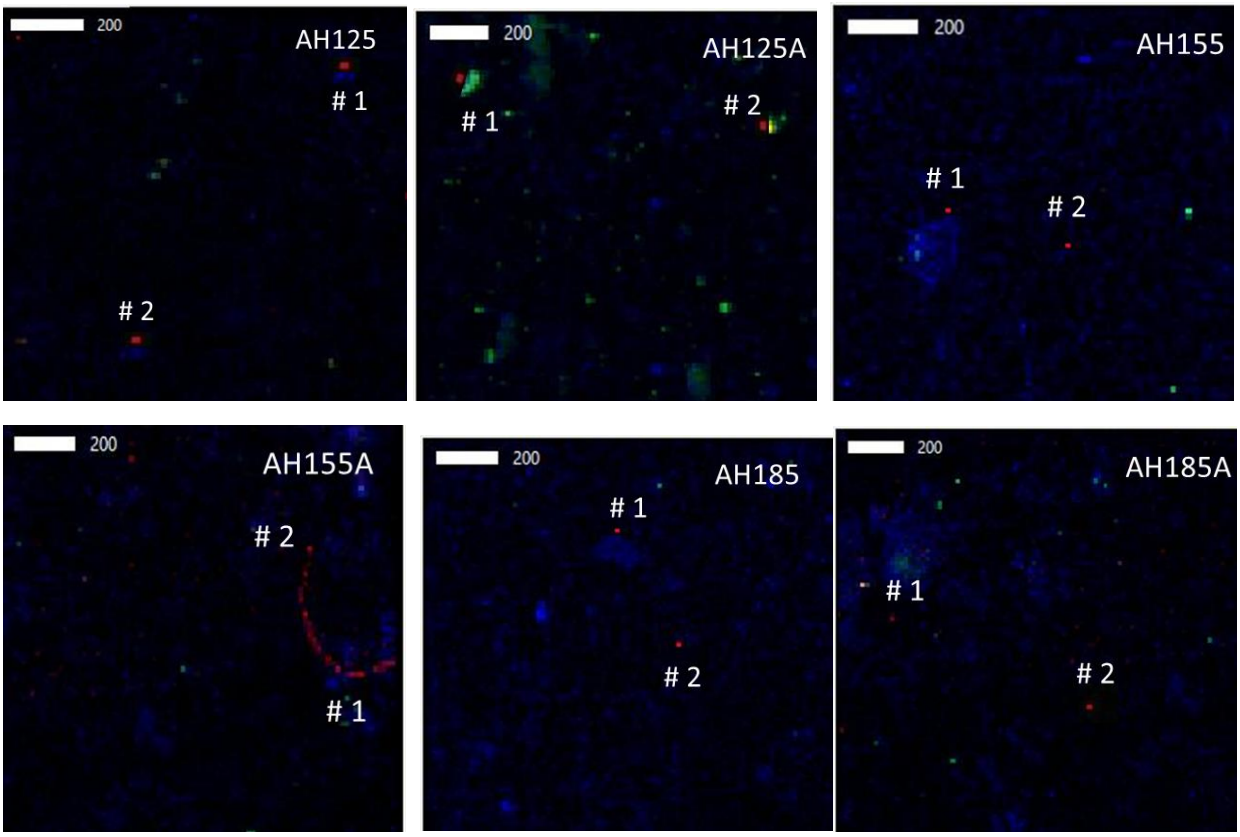

Figure S11. Tricolor μ-XRF images of Cr, Fe, and Si distribution in raw sludge, HT hydrochars, and AD solids. Scale bars are 100 or 200 μm, and the threshold value (arbitrary) in the images were set at 50 (Cr), 1000 (Fe), and 50 (Si). The corresponding Cr K-edge μ-XANES spectra at different hot spots in the μ-XRF images are in Figure S12.

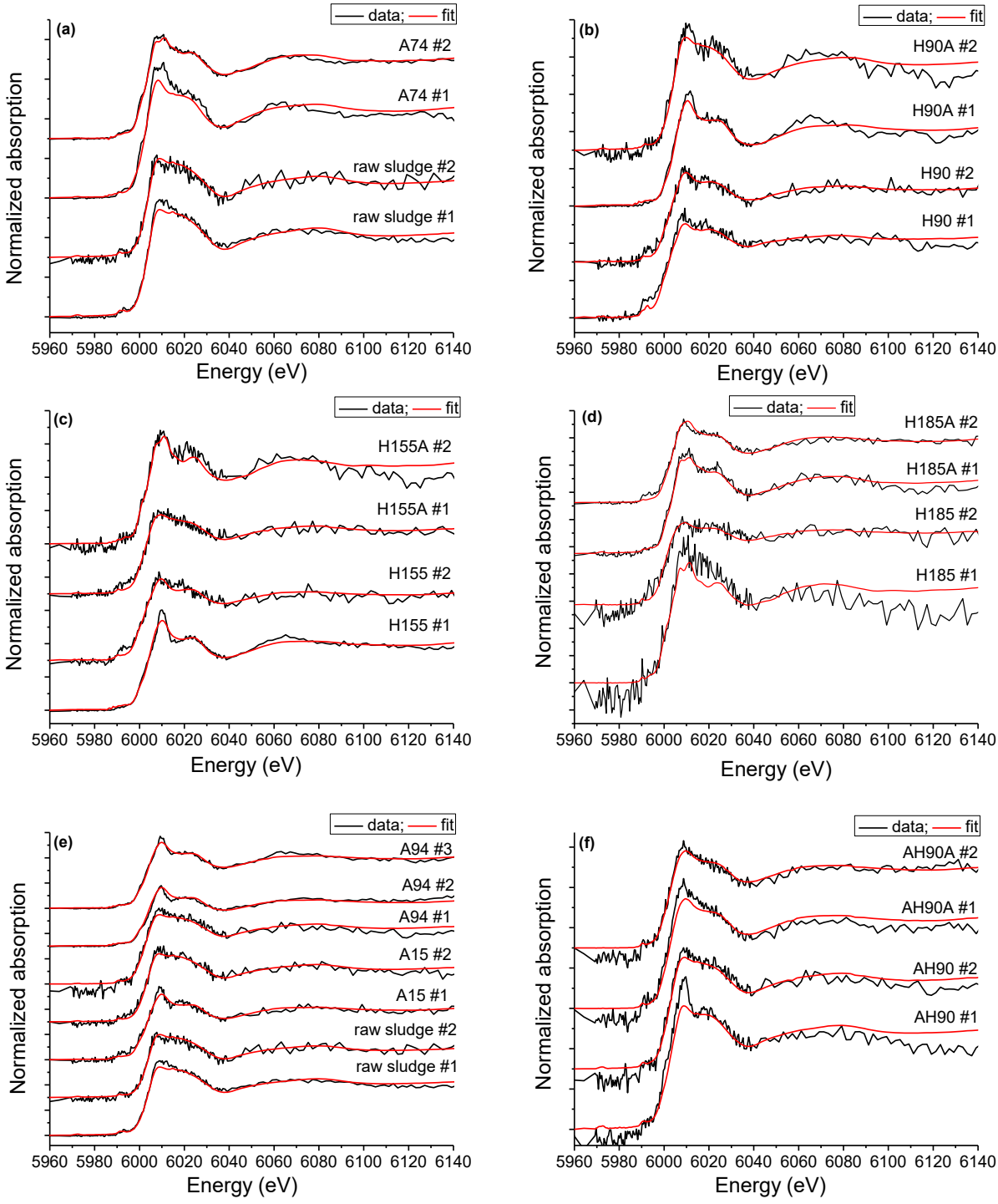
(a)
data; fit
A74 #2
A74 #1
raw sludge #2
raw sludge #1
(b)
H90A #2
H90A #1
H90 #2
H90 #1
(c)
H155A #2
H155A #1
H155 #2
H155 #1
(d)
H185A #2
H185A #1
H185 #2
H185 #1
(e)
A94 #3
A94 #2
A94 #1
A15 #2
A15 #1
raw sludge #2
raw sludge #1
(f)
AH90A #2
AH90A #1
AH90 #2
AH90 #1
Normalized absorption
Energy (eV)
5960 5980 6000 6020 6040 6060 6080 6100 6120 6140

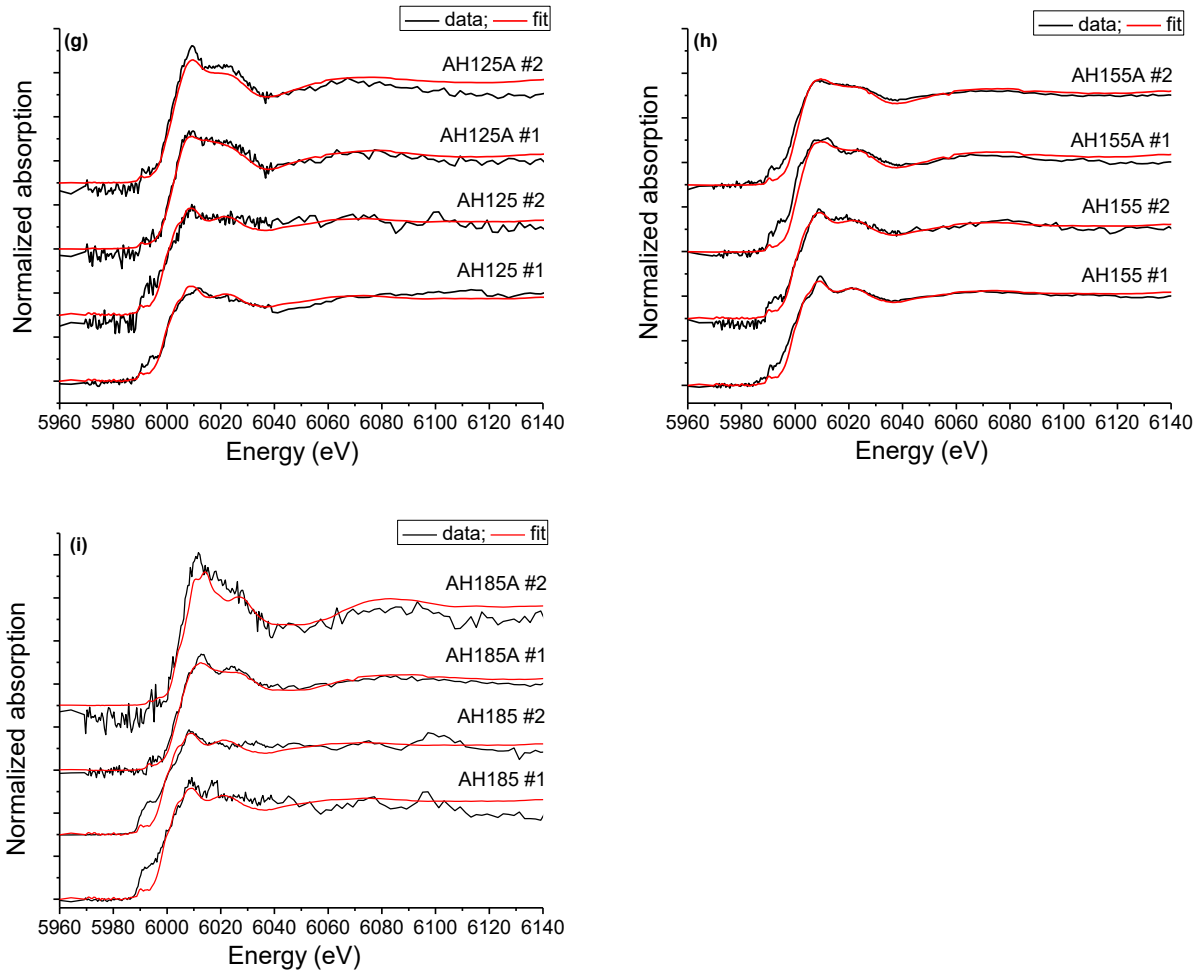

Figure S12. Linear combination fitting (LCF) of Cr K-edge μ-XANES spectra of raw sludge, HT hydrochars, and AD solids from HT-AD and AD-HT-AD systems. Raw and LCF fitted data are shown in black and red lines, respectively.

REFERENCES

1. Mossop, K. F.; Davidson, C. M., Comparison of original and modified BCR sequential extraction procedures for the fractionation of copper, iron, lead, manganese and zinc in soils and sediments. *Anal. Chim. Acta* **2003,** *478*, (1), 111-118.
2. Huang, R.; Zhang, B.; Saad, E. M.; Ingall, E. D.; Tang, Y., Speciation evolution of zinc and copper during pyrolysis and hydrothermal carbonization treatments of sewage sludges. *Water Res.* **2018,** *132*, 260-269.
3. Donner, E.; Howard, D. L.; Jonge, M. D. d.; Paterson, D.; Cheah, M. H.; Naidu, R.; Lombi, E., X-ray absorption and micro X-ray fluorescence spectroscopy investigation of copper and zinc speciation in biosolids. *Environ. Sci. Technol.* **2011,** *45*, (17), 7249-7257.
4. Le Bars, M.; Legros, S.; Levard, C.; Chaurand, P.; Tella, M.; Rovezzi, M.; Browne, P.; Rose, J.; Doelsch, E., Drastic change in zinc speciation during anaerobic digestion and composting: instability of nano-sized zinc sulfide. *Environ. Sci. Technol.* **2018,** *52*, 12987-12996.
5. Lv, J.; Zhang, S.; Luo, L.; Zhang, J.; Yang, K.; Christie, P., Accumulation, speciation and uptake pathway of ZnO nanoparticles in maize. *Environ. Sci.: Nano* **2015,** *2*, (1), 68-77.
6. Aldmour, S. T.; Burke, I. T.; Bray, A. W.; Baker, D. L.; Ross, A. B.; Gill, F. L.; Cibin, G.; Ries, M. E.; Stewart, D. I., Abiotic reduction of Cr (VI) by humic acids derived from peat and lignite: kinetics and removal mechanism. *Environ. Sci. Pollut. Res.* **2019,** *26*, (5), 4717-4729.
7. Saad, E. M.; Sun, J.; Chen, S.; Borkiewicz, O. J.; Zhu, M.; Duckworth, O. W.; Tang, Y., Siderophore and organic acid promoted dissolution and transformation of Cr(III)-Fe(III)-(oxy)hydroxides. *Environ. Sci. Technol.* **2017,** *51*, (6), 3223-3232.
8. Tang, Y.; Michel, F. M.; Zhang, L.; Harrington, R.; Parise, J. B.; Reeder, R. J., Structural properties of the Cr(III)−Fe(III) (Oxy)hydroxide compositional series: insights for a nanomaterial "solid solution". *Chem. Mater.* **2010,** *22*, (12), 3589-3598.
9. Tang, Y.; Elzinga, E. J.; Jae Lee, Y.; Reeder, R. J., Coprecipitation of chromate with calcite: Batch experiments and X-ray absorption spectroscopy. *Geochimica et Cosmochimica Acta* **2007,** *71*, (6), 1480-1493.